Eur. Phys. J. A (2023) 59:22
https://doi.org/10.1140/epja/s10050-023-00929-5

THE EUROPEAN PHYSICAL JOURNAL A

Regular Article - Experimental Physics

The empirical shell gap revisited in light of recent high precision mass spectrometry data

Vladimir Manea[1,a], **Maxime Mougeot**[2,3,4,b], **David Lunney**[1,c]

[1] Université Paris-Saclay, CNRS/IN2P3, IJCLab, 91405 Orsay, France
[2] CERN, 1211 Geneva, Switzerland
[3] Max-Planck-Institut für Kernphysik, 69117 Heidelberg, Germany
[4] University of Jyväskylä, 40014 Jyväskylä, Finland

Received: 1 December 2022 / Accepted: 20 January 2023 / Published online: 10 February 2023

Communicated by N. Alamanos

Abstract We present an updated view on the phenomenon of mutually enhanced magicity based on the current experimental knowledge of atomic masses, including some recent precision measurements performed with the ISOLTRAP mass spectrometer at ISOLDE/CERN. We discuss the trends of the proton and neutron empirical shell gaps computed either in the standard approach, along chains corresponding to magic numbers of protons and neutrons, respectively, or along the neighbouring isotonic chains differing by two nucleon numbers. We show that in the latter case the empirical shell-gap trend is anti-correlated to the one observed along the magic-number chains. We perform a theoretical investigation of the origin of this feature by an analysis of the contributions from the monopole, pairing and quadrupole interactions, focusing on the phenomenon of mutually enhanced magicity. We emphasize the role of quadrupole correlations for explaining the full range of experimental information.

1 Introduction

With the development of precision mass-measurement techniques based on ion traps and storage rings [1], the atomic masses of more than 2400 isotopes have been determined with an uncertainty lower than 100 keV [2]. This significant evolution has refined the features of the mass surface (the locus of all atomic masses as a function of proton and neutron number) to an extent allowing to observe not only its global trend, but also the trends of its derivatives. The latter, expressed as finite differences of atomic masses called mass filters, have played an essential role in studying the different features of nuclear-structure phenomena, such as (in decreasing order of magnitude) shell effects ($\approx$ 5 MeV), pairing gaps ($\approx$ 1 MeV) and quadrupole deformation ($<$ 1 MeV). The enhanced precision has enabled examining more than the average features of these mass filters and the extended range has allowed a broader basis of interpretation.

Of the different mass filters, one of the most widely analyzed and the one that we will give particular attention to in this work is the two-nucleon (neutron or proton) empirical shell gap. It is regarded as an essential piece of experimental information for identifying the so-called nuclear magic numbers and, in relation to a shell or mean-field model of nuclear structure, for quantifying the size of the underlying energy gaps. Such parallels are not without caveats as discussed for example in [3,4], advocating that theory-experiment comparisons should be restricted to the observables themselves. For such comparisons, the two-nucleon shell gap is an attractive benchmark because it is computed only using the masses of even-even nuclei, which are significantly simpler to calculate than their odd counterparts. It is thus not surprising that a lot of experimental effort has gone into extending the knowledge of empirical shell gaps and thus tracing the evolution of magic numbers in exotic nuclei, matched by a comparable theoretical effort, which in the last years has also seen a significant contribution from ab-initio approaches [5–10].

One important experimental feature of the two-neutron empirical shell gap is the so-called "mutually enhanced magicity", namely the fact that moving along a neutron-magic chain the shell gap peaks when crossing a magic number of protons. The same is true for the two-proton empirical shell gap at the crossing of a neutron magic number along a proton-magic isotopic chain. This phenomenon has been

[a] e-mail: vladimir.manea@ijclab.in2p3.fr (corresponding author)
[b] e-mail: maxime.mougeot@cern.ch
[c] e-mail: david.lunney@ijclab.in2p3.fr

observed a few decades ago in the ^{208}Pb region [11] and was explained for ^{208}Pb by [12] using a shell-model framework and quite general arguments, but focusing on the monopole part of the residual interaction, while noting the likely, non-negligible role of multipole correlations. More recently, the phenomenon was described in the framework of a symmetry-restored generator coordinate method (GCM) using a Skyrme interaction (SLy4) [3,13], a crucial role being played by the treatment of quadrupole correlations beyond the mean field (BMF).

With the contribution of precision mass measurements performed at radioactive-ion-beam facilities, evidence for the phenomenon of mutually enhanced magicity has been gathered far beyond the information available at the moment of the original discovery. More recent highlights concern very neutron-rich, doubly magic nuclei in the regions of ^{78}Ni [14] and ^{132}Sn [15–17]. All these measurements suggest that mutually enhanced magicity is a universal phenomenon across the nuclear chart. Furthermore, in one of the more recent studies [18] it was shown that the trend of the neutron empirical shell gap is sensitive to the phenomenon of "enhanced magicity" even when it is computed two neutrons before a magic neutron number. The difference of behaviour for this shifted empirical shell gap is that crossing a proton magic number manifests as a local minimum instead of a maximum. In [18] this was explained as an effect of the same BMF correlations, but without a formal justification. A similar feature was discussed in [19] concerning the neutron shell gap computed two neutrons after a magic number, again relying mostly on empirical analogies.

In this study we analyze precision mass data including some recent measurements from ISOLTRAP [16,18,19] to revisit the phenomenon of mutually enhanced magicity. In particular, we address the universality of the phenomenon, as the arguments brought in the original paper of [12] are relying on single-particle states and residual interactions valid around ^{208}Pb. We begin by reviewing the role of the monopole part of the residual interaction, and discussing in which conditions it explains or not the observed trends of the empirical shell gap. We then go further and address the role of pairing correlations via the seniority model and (by a perturbative analysis) the role of quadrupole correlations. For all the monopole, pairing and quadrupole contributions, we discuss their impact on the trends of the shifted empirical shell gap.

2 Experimental information

The two-nucleon empirical shell gap expresses the drop of the two-nucleon separation energy at the crossing of a magic number (corresponding to the type of nucleon in question). As such, its analogy to a gap in a spectrum of single-particle

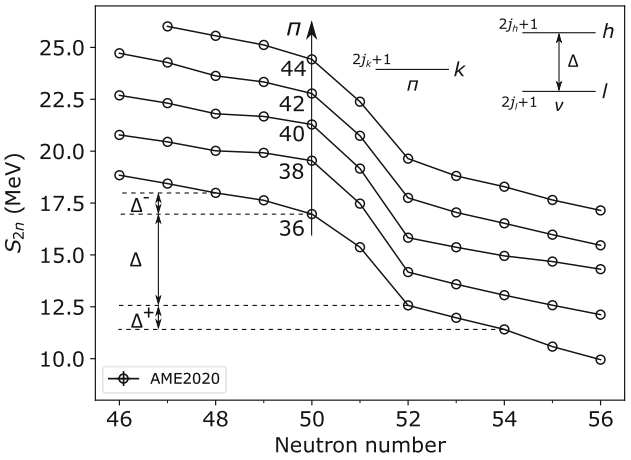

Fig. 1 Experimental two-neutron separation energies S_{2n} from the 2020 Atomic Mass Evaluation [2] as a function of neutron number, for the $Z = 36 - 44$ isotopic chains. Only even Z and N values are considered. The S_{2n} drops defining the two-neutron empirical shell gap at $N = 50$ in the normal (Δ_{2n}) and shifted ($\Delta^{\pm}_{2n}$) variants are marked. The inset presents the simplified model space used for the analysis of the empirical shell-gap trend using the monopole, pairing and quadrupole Hamiltonians. The $2j+1$ degeneracy is explicitly shown for each level. The π axis marks on the S_{2n} plot the Z values of the different chains

energies is immediate. The formal definition of the quantity is:

$$\begin{aligned}\Delta_{2n}(Z, N_0) &= E(Z, N_0 - 2) + E(Z, N_0 + 2) \\ &\quad - 2E(Z, N_0), \\ \Delta_{2p}(Z_0, N) &= E(Z_0 - 2, N) + E(Z_0 + 2, N) \\ &\quad - 2E(Z_0, N), \end{aligned} \tag{1}$$

where $E(Z, N)$ is the (negative) binding energy of the nucleus, the $2n$ and $2p$ subscripts mark the neutron or proton gap, while N_0 and Z_0 correspond to a "magic" number of neutrons or protons, respectively.

The shifted empirical shell gaps mentioned previously, $\Delta^{\pm}_{2n}$ and $\Delta^{\pm}_{2p}$, are defined as:

$$\begin{aligned}\Delta^{\pm}_{2n}(Z, N_0) &= E(Z, N_0 \pm 4) + E(Z, N_0) \\ &\quad - 2E(Z, N_0 \pm 2) \\ \Delta^{\pm}_{2p}(Z_0, N) &= E(Z_0 \pm 4, N) + E(Z_0, N) \\ &\quad - 2E(Z_0 \pm 2, N) \end{aligned} \tag{2}$$

where the $+$ or $-$ superscript denotes the direction in which the definition of the gap is shifted.

In Fig. 1 are shown the experimental two-neutron separation energies as a function of neutron number, for several isotopic chains. The intervals representing the Δ_{2n} and $\Delta^{\pm}_{2n}$ for the magic neutron number $N = 50$ are marked.

In order to start with a global view of the experimental trends, in Fig. 2 we represent the two-neutron empirical

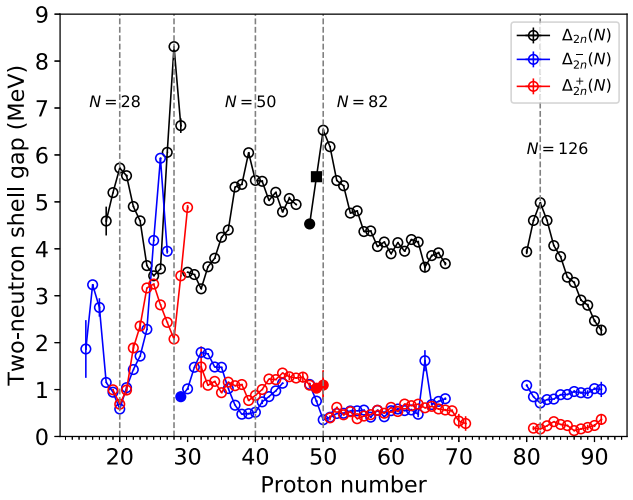

Fig. 2 Two-neutron empirical shell gap computed in the three variants discussed in this work, namely Δ_{2n},Δ^{+}_{2n} and Δ^{-}_{2n}. Data are taken from the AME2016 [20], ISOLTRAP [16,18,19] (full circles) and TITAN [17] (full square). Proton magic numbers are marked by a dashed line

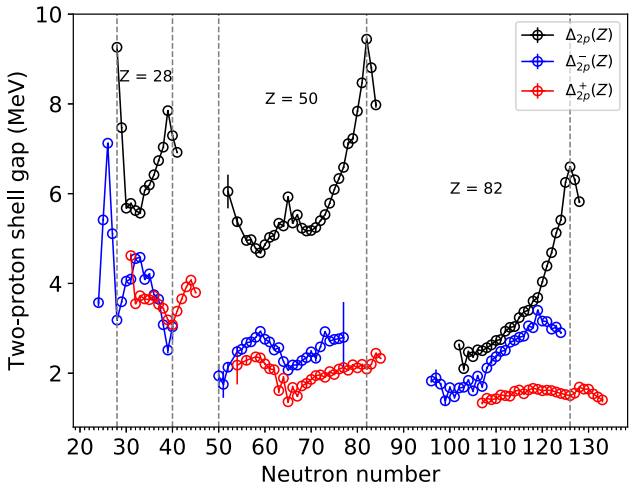

Fig. 3 Two-proton empirical shell gap computed in the three variants discussed in this work, namely Δ_{2p},Δ^{+}_{2p} and Δ^{-}_{2p}. Data are taken from the AME2020 [2]. Neutron magic numbers are marked by a dashed line

shell gap for the magic numbers $N_0 = 28, 50, 82$ and 126, based on data from the Atomic Mass Evaluation. This time the 2016 version of the evaluation [20] is chosen as reference, because it allows emphasizing contributions from more recent measurements performed by ISOLTRAP [16,18,19] and TITAN [17], which are represented in full symbols. The phenomenon of mutually enhanced magicity manifests as the Δ_{2n} peaks observed at the crossing of a magic proton number. One notices quite clearly the minima in Δ^{-}_{2n} at the same proton numbers $Z_0 = 20, 40, 50, 82$, as well as in Δ^{+}_{2n}, where data are available, for $Z_0 = 20, 28, 40$ and perhaps less markedly for $Z_0 = 82$. The (anti-)correlation between the trends of the regular shell gap, on the one hand, and the shifted shell gap, on the other, indicates that a similar nuclear-structure phenomenon should be the dominant cause. A similar picture with similar features is presented for the proton empirical shell gap in Fig. 3 (note that for this figure only data from the most recent AME are shown [2]).

In the following, we will study what is expected for the trends of Δ_{2n} and $\Delta^{\pm}_{2n}$ by considering the effect of the monopole, pairing and quadrupole proton-neutron part of the nuclear Hamiltonian. Taking a perturbative approach, the binding energy of the nuclear system will be described as a sum of independent contributions from the three parts of the interaction:

$$E(Z,N) = E_m + E_{pair} + E_Q, \tag{3}$$

which naturally leads to a similar decomposition of the empirical shell gap (in any variant):

$$\Delta_{2n}(Z,N) = \Delta_{2n,m} + \Delta_{2n,pair} + \Delta_{2n,Q}, \tag{4}$$

all being *a priori* functions of both the proton and the neutron numbers. Although the analysis will focus for simplicity on the neutron empirical shell gap, the results would apply in a similar way to the proton gap.

3 Effect of the monopole Hamiltonian

In a first instance, we will perform the analysis only taking into account the monopole Hamiltonian H_m (as in [12]). Nowadays still a lot of the intuition concerning nuclear-structure evolution with proton and neutron number is based on the effects of the monopole Hamiltonian (see for example the global empirical study of [21] or the more recent review [22]). H_m is written in the second quantization as [23]:

$$\begin{aligned} H_m = &\sum_i \epsilon_i^{\nu} \hat{N}_i^{\nu} + \sum_i \epsilon_i^{\pi} \hat{N}_i^{\pi} + \sum_{ij} \bar{V}_{ij}^{\pi\nu} \hat{N}_i^{\nu} \hat{N}_j^{\pi} \\ &+ \sum_{i,j\geq i} \frac{\hat{N}_i^{\nu}(\hat{N}_j^{\nu} - \delta_{ij})}{1+\delta_{ij}} \bar{V}_{ij}^{\nu\nu} \\ &+ \sum_{i,j\geq i} \frac{\hat{N}_i^{\pi}(\hat{N}_j^{\pi} - \delta_{ij})}{1+\delta_{ij}} \bar{V}_{ij}^{\pi\pi}, \end{aligned} \tag{5}$$

where the indices i, j run over all single-particle states of the shell-model space, ϵ_i are the corresponding single-particle energies, $\hat{N}_i$ are the particle number operators for the states i, $\bar{V}_{ij}$ are the angular-momentum-averaged centroids of the two-body matrix elements (TBME), δ_{ij} is the Kronecker delta and ν, π designate neutron and proton states, respectively. We note that only the diagonal elements of the monopole interaction are considered. Equation (5) shows

that the Hamiltonian H_m does not lead to any mixing of the pure configurations built with the states of the valence-space single-particle basis, but only shifts the binding energy of the system depending on the occupations of these states. The binding energy in this case can be computed analytically, once the interaction parameters are defined.

For simplicity, in the following discussion we will restrict ourselves to a smaller valence space, assuming that protons are filling a single j orbit and that the neutron energy gap is formed between two well defined shells, the occupation of which does not change with the number of protons. The simplification is in fact equivalent to the frozen picture where lower proton and neutron orbits are completely filled and no neutron excitations to higher orbits occur. This is represented in the inset of Fig. 1. While we are limited to the monopole part of the Hamiltonian, this simplification only reduces the size of Eq. (5) without affecting the generality of the result.

In the model space of Fig. 1, the sums in Eq. (5) disappear and H_m is written as:

$$\begin{aligned} H_m = &\epsilon_l^\nu \hat{N}_l^\nu + \epsilon_h^\nu \hat{N}_h^\nu + \epsilon_k^\pi \hat{N}_k^\pi + \bar{V}_{kl}^{\pi\nu} \hat{N}_l^\nu \hat{N}_k^\pi \\ &+ \bar{V}_{kh}^{\pi\nu} \hat{N}_h^\nu \hat{N}_k^\pi + \frac{\hat{N}_l^\nu (\hat{N}_l^\nu - 1)}{2} \bar{V}_{ll}^{\nu\nu} \\ &+ \frac{\hat{N}_h^\nu (\hat{N}_h^\nu - 1)}{2} \bar{V}_{hh}^{\nu\nu} + \hat{N}_l^\nu \hat{N}_h^\nu \bar{V}_{lh}^{\nu\nu} \\ &+ \frac{\hat{N}_k^\pi (\hat{N}_k^\pi - 1)}{2} \bar{V}_{kk}^{\pi\pi} \end{aligned} \tag{6}$$

Taking into account the level degeneracy $2j + 1$, we can now write directly the energy of the nuclei used to compute the empirical shell gap $\Delta_{2n}(Z_0 + N_p, N_0)$, where in our case Z_0 corresponds to an empty k shell and N_0 corresponds to a full l shell and empty h shell. The detailed expressions for the binding energies of the involved nuclei are presented in the Appendix, while here we give only the final expression of the empirical shell gap:

$$\begin{aligned} \Delta_{2n,m} = &2\Delta + 2N_p(\bar{V}_{kh}^{\pi\nu} - \bar{V}_{kl}^{\pi\nu}) - (4j_l - 1)\bar{V}_{ll}^{\nu\nu} \\ &+ 2(2j_l + 1)\bar{V}_{lh}^{\nu\nu} + \bar{V}_{hh}^{\nu\nu}, \end{aligned} \tag{7}$$

where $\Delta = \epsilon_h^\nu - \epsilon_l^\nu$ is the real shell gap in the simplified model and for compactness we have reduced the notation of $\Delta_{2n,m}(Z_0 + N_p, N_0)$ to $\Delta_{2n,m}$.

This result is similar to what was obtained in [12], in which the only term determining a variation of the empirical neutron gap with proton number (at the monopole level) is the difference of the proton-neutron TBME linking the two neutron orbits around the gap and the proton orbit being filled. However, it is clear from Eq. (7) that the gap is maximum at the doubly magic nucleus (Z_0, N_0) with respect to the larger proton numbers only if the term $\bar{V}_{kh}^{\pi\nu} - \bar{V}_{kl}^{\pi\nu}$ is negative, meaning that the neutrons from above the gap are more attracted to the protons than the neutrons from below. Furthermore, a local maximum would be obtained at (Z_0, N_0) only if the difference of monopole TBME changes sign in the proton shell below the magic number. In its most general form, the formula does not exclude obtaining a minimum or neither a minimum, nor a maximum at the magic number, for other values of the proton–neutron interaction.

A maximum separation of the effective single-particle energies (ESPE) defining the neutron gap does indeed occur for $N = 82$ and $N = 126$ at $Z = 50$ and $Z = 82$, respectively, but (in a different region of the nuclear chart) the gap between the neutron ESPEs defining the $N = 50$ shell closure is in fact shrinking towards $Z = 28$ (see discussions in [21,24]) due to the corresponding monopole terms in the Hamiltonian. Experimentally, the mass surface above ^{78}Ni does extrapolate towards a local enhancement of the empirical shell gap at the doubly magic nucleus (see Fig. 3), despite this trend in ESPEs [14,18]. For this latter example, the monopole analysis of Eq. (7) and [12] would not predict a local maximum in Δ_{2n}, contrary to experiment. This brings into discussion the role of correlations beyond the monopole trends, which were not explicitly included in [12].

In order to compute at the monopole level what is expected for Δ_{2n}^-, we need to write also the binding energy of the N_0-4 isotope (see Appendix), leading to a value of Δ_{2n}^-:

$$\Delta_{2n,m}^- = 4\bar{V}_{ll}^{\nu\nu}, \tag{8}$$

while in a similar way one can obtain:

$$\Delta_{2n,m}^+ = 4\bar{V}_{hh}^{\nu\nu}. \tag{9}$$

This means that under the action of a pure-monopole force and assuming a naive filling of the proton and neutron orbits, there is no expected variation of Δ_{2n}^+ or Δ_{2n}^- with proton number. This is also at odds with what is observed experimentally. Both the global trends of the empirical shell gap Δ_{2n} and those of its variants $\Delta_{2n}^\pm$ call for a treatment of the residual interaction beyond the monopole trends.

4 Effect of pairing and of the proton–neutron quadrupole interaction

Unlike the monopole interaction discussed in the previous section, the dependence on Z and N of the binding energy stemming from the pairing and the quadrupole proton–neutron interaction is more difficult to quantify exactly. For the pairing energy, a qualitative view can be gathered from the seniority model for a single degenerate shell, which yields an analytical expression. For the quadrupole correlation energy, an analytical expression valid in the vicinity of closed shells can be obtained using perturbation theory.

Such a study was performed in [25] and applied to the description of the excitation energies of intruder 0^+ states. Later on, a similar approach was integrated in a broader study using the Interacting Boson Model (IBM) of the impact of pairing and quadrupole correlations on the trends of ground-state binding energies [26,27], as well as of the phenomenon of nuclear phase transitions [28–30]. In particular, it was shown in this work that the energy contribution from the quadrupole proton-neutron interaction can be recast as a renormalization of the monopole-pairing interaction between like nucleons [26] and that a monopole pairing interaction leads to a different evolution of the pairing energy along an isotopic chain than a zero-range delta interaction, despite the fact they have similar spectroscopic properties [31]. The approach of [25] has been often used to explain the mechanism behind the emergence of shape coexistence in the vicinity of closed shells [32,33] and has already been applied to describe the excitation energies of intruder 0^+ states in the ^{78}Ni region [34], which will also be a focus of this work.

In the following, we will briefly apply the same technique to the study of empirical shell gaps. First of all, the pairing energy in the ground state of even-N identical nucleons in a single j shell is derived in the seniority model to be [25–27]:

$$E_{pair}(N) = -\frac{G}{4}(2j+1-N+2)N, \tag{10}$$

where G is the pairing interaction strength (a positive value) and it was considered that the ground state corresponds to the seniority $\nu = 0$.

It is clear that the proton pairing energy will not give a contribution to the neutron shell gap in any of the discussed variants Δ_{2n} or $\Delta^{\pm}_{2n}$, because it has no dependence on the neutron number. There will however be a contribution from the neutron pairing energy. The detailed expressions for the involved binding energies are given in the Appendix, but it is straightforward to show that for the schematic model discussed so far, the pairing contribution to Δ_{2n}, assuming an equal neutron pairing strength G for both the lower and the higher shells is:

$$\Delta_{2n,pair} = -G(j_l + j_h - 1), \tag{11}$$

which is always a negative contribution. This is because the open-shell nuclei always have more binding from pairing than the closed-shell ones. Similarly, for the shifted gaps one obtains:

$$\Delta^{\pm}_{2n,pair} = 2G, \tag{12}$$

which is a positive contribution.

With Eqs. (11) and (12) one obtains the result that the pairing interaction simply offsets the shell gap by a constant value, downward for Δ_{2n} and upward for $\Delta^{\pm}_{2n}$, therefore the pairing interaction cannot be responsible for the trends shown in Figs. 2 and 3.

To express the contribution of the quadrupole proton-neutron interaction, we will follow the perturbative approach derived in [25,26]. The operator of the quadrupole proton-neutron interaction is given by:

$$V_{QQ} = \bar{k}\hat{Q}_\pi \cdot \hat{Q}_\nu, \tag{13}$$

where the dot product represents the tensor product of rang zero and $\bar{k}$ is the quadrupole interaction strength. Following [25,26], the binding energy from this interaction, in lowest order of perturbation theory and for the simple case of a single proton orbit j_k and a single neutron orbit j_l, is:

$$E_Q = \frac{2\bar{k}^2}{5\Delta E_{kl}} F(N_p, j_k) F(N_n, j_l) X^\pi_k X^\nu_l, \tag{14}$$

where by E_Q we understand $E_Q(Z_0 + N_p, N_0 + N_n)$ and the X terms are matrix elements of the quadrupole operator:

$$\begin{aligned} X^\pi_k &= \left[\langle (j_k)^2; 0^+ \| Q_\pi \| (j_k)^2; 2^+ \rangle\right]^2, \\ X^\nu_l &= \left[\langle (j_l)^2; 0^+ \| Q_\nu \| (j_l)^2; 2^+ \rangle\right]^2. \end{aligned} \tag{15}$$

and we have made for compactness the following notation:

$$\frac{N_p(2j_k + 1 - N_p)}{2(2j_k - 1)} = F(N_p, j_k), \tag{16}$$

The term X^π_k should be independent of the neutron shell which is being filled, while the term X^ν_l becomes X^ν_h when neutrons are filling the upper shell. The factor ΔE_{kl} is the energy denominator of the perturbation-theory expansion and it too depends on the neutron shell which is being filled. It is a negative quantity, which also gives the sign of E_Q.

With Eq. (14) one can compute the effect of the quadrupole residual interaction on the trends of the ground-state binding energy around doubly magic nuclei, where lowest order perturbation theory is more accurate. In particular, one can compute the binding-energy gain due to the proton-neutron quadrupole interaction for the three variants of Δ_{2n}. The detailed calculations for the involved binding energies are again given in the Appendix, while here we limit ourselves to presenting the final results:

$$\begin{aligned} \Delta_{2n,Q} &= \frac{2\bar{k}^2}{5} F(N_p, j_k) X^\pi_k \left[\frac{X^\nu_l}{\Delta E_{kl}} + \frac{X^\nu_h}{\Delta E_{kh}}\right], \\ \Delta^-_{2n,Q} &= \frac{2\bar{k}^2}{5\Delta E_{kl}} F(N_p, j_k) X^\pi_k X^\nu_l \left(-\frac{4}{2j_l - 1}\right), \\ \Delta^+_{2n,Q} &= \frac{2\bar{k}^2}{5\Delta E_{kh}} F(N_p, j_k) X^\pi_k X^\nu_h \left(-\frac{4}{2j_h - 1}\right). \end{aligned} \tag{17}$$

Equation (17) shows that the quadrupole proton-neutron interaction brings a negative contribution to Δ_{2n} and a positive contribution to $\Delta^{\pm}_{2n}$ (due to the negative sign of the ΔE terms), both varying with the number of valence protons as $F(N_p, j_k)$, a quadratic function of N_p which peaks at the middle of the j_k shell. The fact that the same factor gives the N_p dependence of both $\Delta_{2n,Q}$ and $\Delta^{\pm}_{2n,Q}$ determines a correlation between the two quantities, with the former reaching a maximum and the latter reaching a minimum for a closed proton shell.

By using Eq. (4), we can now express the values of Δ_{2n} and $\Delta^{\pm}_{2n}$ considering all contributions from the monopole, pairing and quadrupole interactions:

$$
\begin{aligned}
\Delta_{2n} =& 2\Delta + 2N_p(\bar{V}^{\pi\nu}_{kh} - \bar{V}^{\pi\nu}_{kl}) + V^{\nu\nu} \\
& - \frac{2\bar{k}^2}{5} F(N_p, j_k) X^{\pi}_k \left[\frac{X^{\nu}_l}{|\Delta E_{kl}|} + \frac{X^{\nu}_h}{|\Delta E_{kh}|} \right], \\
\Delta^{-}_{2n} =& 4\bar{V}^{\nu\nu}_{ll} + 2G + \frac{2\bar{k}^2}{5|\Delta E_{kl}|} \\
& \times \left(\frac{4}{2j_l - 1} \right) F(N_p, j_k) X^{\pi}_k X^{\nu}_l, \\
\Delta^{+}_{2n} =& 4\bar{V}^{\nu\nu}_{hh} + 2G + \frac{2\bar{k}^2}{5|\Delta E_{kh}|} \\
& \times \left(\frac{4}{2j_h - 1} \right) F(N_p, j_k) X^{\pi}_k X^{\nu}_h,
\end{aligned}
\tag{18}
$$

where we have also made the quadrupole terms explicitly positive in order to clearly illustrate in the formula whether they give a negative or a positive contribution. The term $V^{\nu\nu} = -(4j_l - 1)\bar{V}^{\nu\nu}_{ll} + 2(2j_l + 1)\bar{V}^{\nu\nu}_{lh} + \bar{V}^{\nu\nu}_{hh} - G(j_l + j_h - 1)$ groups all the monopole neutron-neutron interactions in Eq. (7) that do not depend on N_p and the contribution of the pairing interaction.

Coming back to the expression of the usual shell gap Δ_{2n}, we remark again that the $2N_p(\bar{V}^{\pi\nu}_{kh} - \bar{V}^{\pi\nu}_{kl})$ term originating in the monopole interaction can determine a peak at the crossing of a proton magic number only if the difference $\bar{V}^{\pi\nu}_{kh} - \bar{V}^{\pi\nu}_{kl}$ is negative above the magic number and changes sign below, which is not generally true. In addition, this term does not explain a correlation between the Δ_{2n} and $\Delta^{\pm}_{2n}$, as it is only present in the expression of Δ_{2n}. On the other hand, the term originating in the quadrupole proton-neutron interaction has the correct sign irrespective of the specific shell configuration and produces the experimentally observed correlation with $\Delta^{\pm}_{2n}$. This is in agreement with the already mentioned conclusions of Bender et al. [3,13] which describe the phenomenon of mutually enhanced magicity by the effect of BMF quadrupole correlations.

We note that the assumptions made in this analysis break down far from doubly magic nuclei, where the perturbative and the single-shell approach are no longer correct. A more realistic approach would take into account the occupation of several subshells by the valence protons and neutrons, which would smooth out the quadratic behavior of the quadrupole energy, in agreement with what is observed experimentally. This simplified approach is however enough in order to give a qualitative explanation of the observed trends of the empirical shell gap.

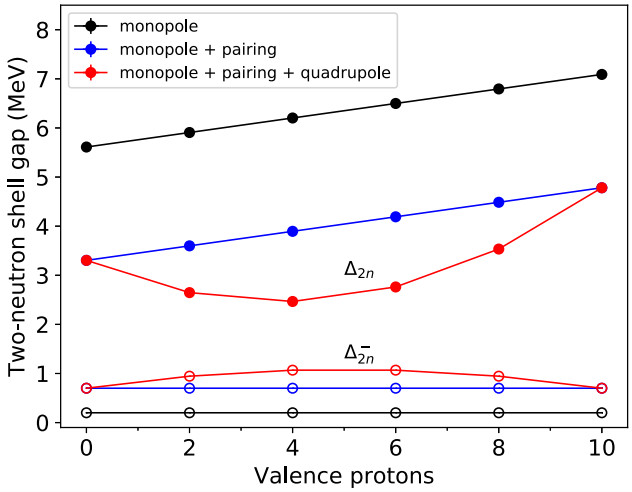

Fig. 4 Trends of the two-neutron empirical shell gap with proton number in its normal Δ_{2n} (filled symbols) and shifted Δ^{-}_{2n} variant (open symbols) for an illustrative analytical model built on the simple valence space of Fig. 1 (considering the total angular momentum of the proton orbital $j_k = 9/2$) and defining the total binding energy as the sum of monopole Eq. (6), pairing, Eq. (10) and quadrupole contributions, Eq. (14), added as shown in Eq. (3). The different curves give the trends corresponding to only monopole (black), monopole + pairing (blue) and full monopole + pairing + quadrupole contributions (red)

In order to better illustrate the trends resulting from the different contributions discussed in this section, in Fig. 4 we present the two-neutron empirical shell gap obtained in the simplified model built on the level scheme of Fig. 1. Both the normal Δ_{2n} and the shifted variant Δ^{-}_{2n} are shown.

The total binding energy is calculated as the sum of the three contributions in Eq. (3) (see red circles) and each contribution is calculated as discussed in this section. The plot thus illustrates the results of Eq. (18). The abscissa of the plot shows the number of valence protons and the number of neutrons considered is $2j_l + 1$, thus corresponding to a closed neutron shell. The zero on the abscissa corresponds to a proton shell closure and thus a doubly magic nucleus. The parameters of the model are loosely based on fits to the ^{78}Ni region, with a $Z_0 = 28$ and $N_0 = 40$ proton/neutron cores, respectively. Because a long proton shell is required for observing the trends, the j_k of the proton orbit is nevertheless considered to be $j_k = 9/2$, as if the $f_{5/2}$ and $p_{3/2}$ orbits between $Z = 28$ and $Z = 38$ formed only one degenerate shell. This simplification is for illustration purposes only. The proton-neutron monopole interactions are fixed based

on the slopes of the one-neutron separation energies along $N = 49$ and $N = 51$. The neutron-neutron and proton-proton monopole matrix elements are fixed for simplicity to 0.05 MeV for nucleons in the same shell and 0 for nucleons across the shell gap. The former are average values of typical monopole matrix elements for like nucleons. The pairing interaction G is fixed to a unique value (for both protons and neutrons) of 0.25 MeV, while the k strength of the quadrupole interaction is fixed to -0.15 MeV. Finally, the parameters of the perturbative expansion $|\Delta E|$ are fixed to 2.5 MeV and the X^{π} and X^{ν} squared integrals are fixed to values ≈ 11, as calculated in [26,35].

Figure 4 presents, apart from the trends of the empirical shell gap from the sum of monopole, pairing and quadrupole contributions, also the trends from only the monopole or only the monopole plus pairing terms. The figure confirms that the monopole interaction leads to a monotonic trend in Δ_{2n} and a flat trend in Δ^{-}_{2n} (black points), while the pairing interaction only shifts the two trends (downward for Δ_{2n} and upward for Δ^{-}_{2n}). It is only the quadrupole interaction that adds the quadratic dependence, producing a local maximum at the proton shell closures (0 and 10 on the axis) for Δ_{2n}, corresponding to local minima in Δ^{-}_{2n}. The particular fitting of monopole proton-neutron interactions (appropriate to the ^{78}Ni region) also leads to a situation where the monopole interaction by itself cannot produce the phenomenon of locally enhanced magicity at 0 valence protons, however the local enhancement emerges naturally from the quadratic contribution of the quadrupole interaction.

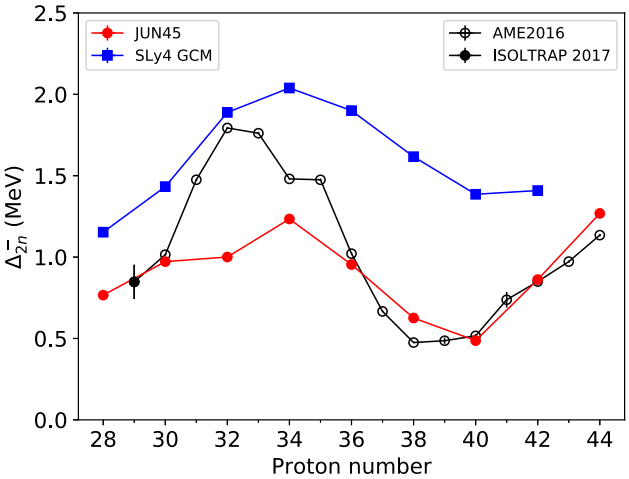

Fig. 5 Experimental Δ^{-}_{2n} values for the $N = 50$ isotones compared to theoretical models. The data are from the AME2016 [20] and the ISOLTRAP work on n-rich copper isotopes [18]. The theoretical results represented with red circles are from shell-model calculations using the full JUN45 interaction [36]. The results represented with blue squares are self-consistent mean-field calculations of [13], using the beyond-mean-field framework based on the generator coordinate method

5 Comparison to state-of-the-art models

In order to compare experimental data to realistic nuclear models, in Fig. 5 we show the experimental Δ^{-}_{2n} values of the $N = 50$ isotones from the AME2016 [20] and [18] and we present for comparison also theoretical values obtained in the shell-model and the beyond-mean-field frameworks. One notices that the latest value measured by ISOLTRAP for Cu ($Z = 29$) continues the downward trend towards ^{78}Ni, supporting its doubly-magic character.

The shell model calculations are performed using the Antoine code [23,37] (and verified with the NuShellX@MSU code [38]) and the JUN45 interaction [36], which spans for both protons and neutrons the valence space $1f_{5/2}$, $2p_{3/2}$,$2p_{1/2}$,$1g_{9/2}$. No valence-space restrictions or truncations are applied. The theoretical curve of Fig. 5 shows a good agreement to experiment, confirming that the features of Δ^{-}_{2n} can be reproduced if multipole valence-space correlations are allowed.

The BMF calculations presented in Fig. 5 are the ones of [13], using a symmetry-restored generator coordinate method (GCM). This approach allows including not only the correlation energy from static quadrupole deformation, but also the one resulting from quadrupole shape fluctuations. One notices again a good comparison to experiment, underlining the fact that the BMF approach of [13] does not only describe the mutually enhanced magicity in the normal shell gap, but also the finer effect observed in the shifted one.

Conclusions

In this work, we reanalysed the global trends of the two-nucleon empirical shell gap in the vicinity of doubly magic nuclei, in particular the phenomenon of mutually enhanced magicity. We have defined a version of the two-nucleon empirical shell gap shifted by two neutrons/protons along the computation axis, called $\Delta^{\pm}_{2n}$ and $\Delta^{\pm}_{2p}$. We have illustrated that the trends of this filter with respect to the complementary nucleon number are well correlated to those of the regular empirical shell gap (Δ_{2n} and Δ_{2p}) but exhibiting local minima where the local maxima of the latter are found. The new filter can prove useful to study the evolution of a magic number when not enough data are available to compute the regular shell gap, as in the case of [18].

The explanation of the phenomenon of mutually enhanced magicity, given in [12] in terms of the monopole Hamiltonian, was revisited. We show that the monopole interactions cannot alone explain the apparent universality of the phenomenon and cannot at all explain the trends of shifted shell gap. We show following the work of [25–27] that the inclusion of the quadrupole–quadrupole interaction is neces-

sary and allows explaining the local maxima/ minima in the regular/shifted shell gap, respectively, as well as their anti-correlation. We illustrate this for the case of Δ^{-}_{2n} at $N = 50$ using the shell-model [23,36–38] and the beyond-mean-field [13] approaches.

It is apparent from this work that the trends of the mass surface possess more features than the well established signatures of nuclear-structure phenomena. High-precision mass measurements are thus necessary in order to supply nuclear models with the full set of phenomena that binding energies are sensitive to.

Acknowledgements The authors would like to thank Kris Heyde for valuable exchanges on some of the theoretical aspects involved in the preparation of the manuscript.

Data Availability Statement This manuscript has no associated data or the data will not be deposited. [Authors' comment: The experimental data used in the article are tabulated in the Atomic Mass Evaluation (versions 2016 and 2020), or in newer publications, as cited where appropriate. The theoretical values used for Fig. 5 are either tabulated in Ref. [13], or computed using the shell-model codes Antoine [37] and NuShellX [38], with standard input files for the used interaction.]

Appendix A

In this Appendix we present detailed expressions for the binding-energy terms appearing in the different equations for Δ_{2n} and $\Delta^{\pm}_{2n}$, when considering the monopole Hamiltonian or the pairing and quadrupole-quadrupole residual interactions. We will denote these energies as $E_m(Z, N)$, $E_{pair}(Z, N)$, $E_Q(Z, N)$, respectively, and express the nucleon numbers with respect to a doubly magic nucleus (Z_0, N_0) as:

$$E(Z, N) = E(Z_0 + N_p, N_0 + N_n), \tag{A1}$$

with N_n either positive or negative and N_p only positive in the simplified model space. Finally, for compactness we will drop the Z_0 and N_0 from every function $E(Z_0 + N_p, N_0 + N_n)$ and cast N_p, N_n as superscripts, giving E^{N_p,N_n}. This simplification will be systematically applied to all binding-energy contributions given below.

With this convention and using Eq. (6), one can write at the monopole level the energies of the nuclei used to compute the different variants of the empirical shell gap:

$$\begin{aligned}
E_m^{N_p,-4} &= (2j_l - 3)\epsilon_l^{\nu} + N_p\epsilon_k^{\pi} + N_p(2j_l - 3)\bar{V}_{kl}^{\pi\nu} \\
&\quad + (j_l - 2)(2j_l - 3)\bar{V}_{ll}^{\nu\nu} \\
&\quad + \frac{N_p(N_p - 1)}{2}\bar{V}_{kk}^{\pi\pi} \\
E_m^{N_p,-2} &= (2j_l - 1)\epsilon_l^{\nu} + N_p\epsilon_k^{\pi} + N_p(2j_l - 1)\bar{V}_{kl}^{\pi\nu} \\
&\quad + (j_l - 1)(2j_l - 1)\bar{V}_{ll}^{\nu\nu} \\
&\quad + \frac{N_p(N_p - 1)}{2}\bar{V}_{kk}^{\pi\pi} \\
E_m^{N_p,0} &= (2j_l + 1)\epsilon_l^{\nu} + N_p\epsilon_k^{\pi} + N_p(2j_l + 1)\bar{V}_{kl}^{\pi\nu} \\
&\quad + j_l(2j_l + 1)\bar{V}_{ll}^{\nu\nu} \\
&\quad + \frac{N_p(N_p - 1)}{2}\bar{V}_{kk}^{\pi\pi} \\
E_m^{N_p,2} &= (2j_l + 1)\epsilon_l^{\nu} + 2\epsilon_h^{\nu} + N_p\epsilon_k^{\pi} + 2N_p\bar{V}_{kh}^{\pi\nu} \\
&\quad + N_p(2j_l + 1)\bar{V}_{kl}^{\pi\nu} + j_l(2j_l + 1)\bar{V}_{ll}^{\nu\nu} \\
&\quad + \bar{V}_{hh}^{\nu\nu} + 2(2j_l + 1)\bar{V}_{lh}^{\nu\nu} \\
&\quad + \frac{N_p(N_p - 1)}{2}\bar{V}_{kk}^{\pi\pi} \\
E_m^{N_p,4} &= (2j_l + 1)\epsilon_l^{\nu} + 4\epsilon_h^{\nu} + N_p\epsilon_k^{\pi} + 4N_p\bar{V}_{kh}^{\pi\nu} \\
&\quad + N_p(2j_l + 1)\bar{V}_{kl}^{\pi\nu} + j_l(2j_l + 1)\bar{V}_{ll}^{\nu\nu} \\
&\quad + 6\bar{V}_{hh}^{\nu\nu} + 4(2j_l + 1)\bar{V}_{lh}^{\nu\nu} \\
&\quad + \frac{N_p(N_p - 1)}{2}\bar{V}_{kk}^{\pi\pi}
\end{aligned} \tag{A2}$$

For the seniority-type pairing interaction, we will only give below the values of the neutron pairing energy. The reason is that in Eq. (11) we present the neutron empirical shell gap, which is computed using nuclei having the same number of protons and hence (in the presented model) the same proton pairing energy, which cancels out. Thus, Eq. (10) leads to the following neutron pairing energies:

$$\begin{aligned}
E_{pair}^{N_p,-4} &= -\frac{3}{2}G_l(2j_l - 3), \\
E_{pair}^{N_p,-2} &= -G_l(2j_l - 1), \\
E_{pair}^{N_p,0} &= -\frac{1}{2}G_l(2j_l + 1), \\
E_{pair}^{N_p,2} &= -\frac{1}{2}G_l(2j_l + 1) - \frac{1}{2}G_h(2j_h + 1), \\
E_{pair}^{N_p,4} &= -\frac{1}{2}G_l(2j_l + 1) - G_h(2j_h - 1),
\end{aligned} \tag{A3}$$

where we have allowed for the pairing interaction in the lower neutron shell G_l to be different from the one in the higher shell G_h. One should note that a contribution from the pairing interaction remains even when the lower neutron shell is completely full.

With Eqs. (14) and (16), it is also possible to compute the energies of the same nuclei by considering only the quadrupole-quadrupole part of the nuclear Hamiltonian.

$$\begin{aligned}
E_Q^{N_p,-4} &= \frac{2\bar{k}^2}{5\Delta E_{kl}}F(N_p, j_k)\frac{2(2j_l - 3)}{2j_l - 1}X_k^{\pi}X_l^{\nu}, \\
E_Q^{N_p,-2} &= \frac{2\bar{k}^2}{5\Delta E_{kl}}F(N_p, j_k)X_k^{\pi}X_l^{\nu}, \\
E_Q^{N_p,0} &= 0,
\end{aligned}$$

$$E_Q^{N_p,2} = \frac{2\bar{k}^2}{5\Delta E_{kh}} F(N_p, j_k) X_k^\pi X_h^\nu,$$
$$E_Q^{N_p,4} = \frac{2\bar{k}^2}{5\Delta E_{kh}} F(N_p, j_k) \frac{2(2j_h - 3)}{2j_h - 1} X_k^\pi X_h^\nu. \quad \text{(A4)}$$

In this case, contrary to the pairing interaction, the quadrupole interaction energy vanishes both for an empty and for a full neutron shell, therefore above the shell gap only the quadrupole-quadrupole interaction of neutrons in j_h plays a role.

References

1. T. Yamaguchi, H. Koura, Y.A. Litvinov, M. Wang, Masses of exotic nuclei. Prog. Part. Nucl. Phys. **120**, 103882 (2021). https://doi.org/10.1016/j.ppnp.2021.103882
2. M. Wang, W.J. Huang, F.G. Kondev, G. Audi, S. Naimi, The AME 2020 atomic mass evaluation (II). Tables, graphs and references. Chinese Phys. C 45(3), 030003 (2021). https://doi.org/10.1088/1674-1137/abddaf
3. M. Bender, G.F. Bertsch, P.-H. Heenen, Collectivity-induced quenching of signatures for shell closures. Phys. Rev. C **78**, 54312 (2008). https://doi.org/10.1103/PhysRevC.78.054312
4. T. Duguet, H. Hergert, J.D. Holt, V. Somà, Nonobservable nature of the nuclear shell structure: Meaning, illustrations, and consequences. Phys. Rev. C **92**(3), 34313 (2015). https://doi.org/10.1103/PhysRevC.92.034313
5. T. Otsuka, T. Suzuki, J.D. Holt, A. Schwenk, Y. Akaishi, Three-Body Forces and the Limit of Oxygen Isotopes. Phys. Rev. Lett. **105**, 32501 (2010). https://doi.org/10.1103/PhysRevLett.105.032501
6. K. Hebeler, J.D. Holt, J. Menéndez, A. Schwenk, Nuclear Forces and Their Impact on Neutron-Rich Nuclei and Neutron-Rich Matter. Annu. Rev. Nucl. Part. Sci. **65**(1), 457–484 (2015). https://doi.org/10.1146/annurev-nucl-102313-025446
7. G. Hagen, G.R. Jansen, T. Papenbrock, Structure of ^{78}Ni from First-Principles Computations. Phys. Rev. Lett. **117**(17), 172501 (2016). https://doi.org/10.1103/PhysRevLett.117.172501
8. S.R. Stroberg, A. Calci, H. Hergert, J.D. Holt, S.K. Bogner, R. Roth, A. Schwenk, Nucleus-dependent valence-space approach to nuclear structure. Phys. Rev. Lett. **118**, 32502 (2017). https://doi.org/10.1103/PhysRevLett.118.032502
9. T.D. Morris, J. Simonis, S.R. Stroberg, C. Stumpf, G. Hagen, J.D. Holt, G.R. Jansen, T. Papenbrock, R. Roth, A. Schwenk, Structure of the Lightest Tin Isotopes. Phys. Rev. Lett. **120**(15), 152503 (2018). https://doi.org/10.1103/PhysRevLett.120.152503
10. H. Hergert, A guided tour of ab initio nuclear many-body theory. Frontiers in Physics **8** (2020). https://doi.org/10.3389/fphy.2020.00379
11. K.-H. Schmidt, D. Vermeulen, In: Nolen, J.A., Benenson, W. (eds.) Mutual Support of Magicities, pp. 119–128. Springer, Boston, MA (1980). https://doi.org/10.1007/978-1-4684-3716-4_13
12. N. Zeldes, T.S. Dumitrescu, H.S. Köhler, Mutual support of magicities and residual effective interactions near ^{208}Pb. Nucl. Phys. A **399**(1), 11–50 (1983). https://doi.org/10.1016/0375-9474(83)90592-4
13. M. Bender, G.F. Bertsch, P.-H. Heenen, Global study of quadrupole correlation effects. Phys. Rev. C **73**, 34322 (2006). https://doi.org/10.1103/PhysRevC.73.034322
14. ...R.N. Wolf, D. Beck, K. Blaum, C. Böhm, C. Borgmann, M. Breitenfeldt, N. Chamel, S. Goriely, F. Herfurth, M. Kowalska, S. Kreim, D. Lunney, V. Manea, E. Minaya Ramirez, S. Naimi, D. Neidherr, M. Rosenbusch, L. Schweikhard, J. Stanja, F. Wienholtz, K. Zuber, Plumbing neutron stars to new depths with the binding energy of the exotic nuclide ^{82}Zn. Phys. Rev. Lett. **110**, 41101 (2013). https://doi.org/10.1103/PhysRevLett.110.041101
15. M. Dworschak, G. Audi, K. Blaum, P. Delahaye, S. George, U. Hager, F. Herfurth, A. Herlert, A. Kellerbauer, H.J. Kluge, D. Lunney, L. Schweikhard, C. Yazidjian, Restoration of the N=82 shell gap from direct mass measurements of ^{132,134}Sn. Phys. Rev. Lett. **100**(7), 072501 (2008). https://doi.org/10.1103/PhysRevLett.100.072501
16. V. Manea, J. Karthein, D. Atanasov, M. Bender, K. Blaum, T.E. Cocolios, S. Eliseev, A. Herlert, J.D. Holt, W.J. Huang, Y.A. Litvinov, D. Lunney, J. Menéndez, M. Mougeot, D. Neidherr, L. Schweikhard, A. Schwenk, J. Simonis, A. Welker, F. Wienholtz, K. Zuber, First Glimpse of the N=82 Shell Closure below Z=50 from Masses of Neutron-Rich Cadmium Isotopes and Isomers. Phys. Rev. Lett. **124**(9), 092502 (2020). https://doi.org/10.1103/PhysRevLett.124.092502
17. C. Izzo, J. Bergmann, K.A. Dietrich, E. Dunling, D. Fusco, A. Jacobs, B. Kootte, G. Kripkó-Koncz, Y. Lan, E. Leistenschneider, E.M. Lykiardopoulou, I. Mukul, S.F. Paul, M.P. Reiter, J.L. Tracy, C. Andreoiu, T. Brunner, T. Dickel, J. Dilling, I. Dillmann, G. Gwinner, D. Lascar, K.G. Leach, W.R. Plaß, C. Scheidenberger, M.E. Wieser, A.A. Kwiatkowski, Mass measurements of neutron-rich indium isotopes for r-process studies. Phys. Rev. C **103**, 025811 (2021). https://doi.org/10.1103/PhysRevC.103.025811
18. A. Welker, N.A.S. Althubiti, D. Atanasov, K. Blaum, T.E. Cocolios, F. Herfurth, S. Kreim, D. Lunney, V. Manea, M. Mougeot, D. Neidherr, F. Nowacki, A. Poves, M. Rosenbusch, L. Schweikhard, F. Wienholtz, R.N. Wolf, K. Zuber, Binding Energy of ^{79}Cu: Probing the Structure of the Doubly Magic ^{78}Ni from Only One Proton Away. Phys. Rev. Lett. **119**(19), 192502 (2017). https://doi.org/10.1103/PhysRevLett.119.192502
19. M. Mougeot, D. Atanasov, J. Karthein, R.N. Karthein, R.N. Wolf, P. Ascher, K. Blaum, K. Chrysalidis, G. Hagen, J.D. Holt, W.J. Huang, G.R. Jasen, I. Kulikov, Y.A. Litvinov, D. Lunney, V. Manea, T. Miyagi, T. Papenbrock, L. Schweikhard, A. Schwenk, T. Steinsberger, S.R. Stroberg, Z.H. Sun, A. Welker, F. Wienholtz, S.G. Wilkins, K. Zuber, Mass measurements of $^{99-101}$In challenge ab initio nuclear theory of the nuclide ^{100}Sn. Nature Phys. **17**, 1099 (2021). https://doi.org/10.1038/s41567-021-01326-9
20. Wang, M., Audi, G., Kondev, F.G., Huang, W.J., Naimi, S., Xu, X., : The AME2016 atomic mass evaluation (II). Tables, graphs and references. Chinese Phys. C 41(3), 30003 (2017)
21. O. Sorlin, M.-G. Porquet, Nuclear magic numbers: New features far from stability. Progr. Part. Nucl. Phys. **61**, 602 (2008). https://doi.org/10.1016/j.ppnp.2008.05.001
22. T. Otsuka, A. Gade, O. Sorlin, T. Suzuki, Y. Utsuno, Evolution of shell structure in exotic nuclei. Rev. Mod. Phys. **92**, 015002 (2020). https://doi.org/10.1103/RevModPhys.92.015002
23. E. Caurier, G. Martínez-Pinedo, F. Nowacki, A. Poves, A.P. Zuker, The shell model as a unified view of nuclear structure. Rev. Mod. Phys. **77**, 427 (2005). https://doi.org/10.1103/RevModPhys.77.427
24. M.-G. Porquet, O. Sorlin, Evolution of the $N = 50$ gap from $Z = 30$ to $Z = 38$ and extrapolation toward ^{78}Ni. Phys. Rev. C **85**(1), 14307 (2012). https://doi.org/10.1103/PhysRevC.85.014307
25. K. Heyde, J. Jolie, J. Moreau, J. Ryckebusch, M. Waroquier, P. Van Duppen, M. Huyse, J.L. Wood, A shell-model description of 0^+ intruder states in even-even nuclei. Nucl. Phys. A **466**(2), 189–226 (1987). https://doi.org/10.1016/0375-9474(87)90439-8
26. R. Fossion, C. De Coster, J.E. Garcia-Ramos, K. Heyde, Proton-neutron quadrupole interactions: An effective contribution to the pairing field. Phys. Rev. C **65**(4), 44309 (2002). https://doi.org/10.1103/PhysRevC.65.044309

27. R. Fossion, C.D. Coster, J.E. Garcia-Ramos, T. Werner, K. Heyde, Nuclear binding energies: Global collective structure and local shell-model correlations. Nucl. Phys. A **697**(3), 703–747 (2002). https://doi.org/10.1016/S0375-9474(01)01270-2
28. J.E. Garcia Ramos, C. DeCoster, R. Fossion, K. Heyde, Two-neutron separation energies, binding energies and phase transitions in the interacting boson model. Nucl. Phys. A **688**, 735 (2001). https://doi.org/10.1016/S0375-9474(00)00592-3
29. S. Schwarz, F. Ames, G. Audi, D. Beck, G. Bollen, C. DeCoster, J. Dilling, O. Engels, R. Fossion, J.-E. Garcia-Ramos, S. Henry, F. Herfurth, K. Heyde, A. Kellerbauer, H.-J. Kluge, A. Kohl, E. Lamour, D. Lunney, I. Martel, R.B. Moore, M. Oinonen, H. Raimbault-Hartmann, C. Scheidenberger, G. Sikler, J. Szerypo, C. Weber, Accurate masses of neutron-deficient nuclides close to $Z = 82$. Nucl. Phys. A **693**, 533 (2001). https://doi.org/10.1016/S0375-9474(01)00881-8
30. J.E. Garcia-Ramos, K. Heyde, R. Fossion, V. Hellemans, S. De Baerdemacker, A theoretical description of energy spectra and two-neutron separation energies for neutron-rich zirconium isotopes. Eur. Phys. J. A **26**(2), 221–225 (2005). https://doi.org/10.1140/epja/i2005-10176-1
31. K. Heyde, R. Fossion, J.E. Garcia-Ramos, C. De Coster, R.F. Casten, Differences between pairing and zero-range effective interactions for nuclear binding energies. Eur. Phys. J. A **13**(4), 401–403 (2002). https://doi.org/10.1140/epja/iepja1347
32. K. Heyde, J.L. Wood, Shape coexistence in atomic nuclei. Rev. Mod. Phys. **83**, 1467–1521 (2011). https://doi.org/10.1103/RevModPhys.83.1467
33. P.E. Garrett, M. Zielinska, E. Clément, An experimental view on shape coexistence in nuclei. Prog. Part. Nucl. Phys. **124**, 103931 (2022). https://doi.org/10.1016/j.ppnp.2021.103931
34. A. Gottardo, D. Verney, C. Delafosse, F. Ibrahim, B. Roussière, C. Sotty, S. Roccia, C. Andreoiu, C. Costache, M.-C. Delattre, I. Deloncle, A. Etilé, S. Franchoo, C. Gaulard, J. Guillot, M. Lebois, M. MacCormick, N. Marginean, R. Marginean, I. Matea, C. Mihai, I. Mitu, L. Olivier, C. Portail, L. Qi, L. Stan, D. Testov, J. Wilson, D.T. Yordanov, First evidence of shape coexistence in the ^{78}Ni region: Intruder 0_2^+ state in ^{80}Ge. Phys. Rev. Lett. **116**, 182501 (2016). https://doi.org/10.1103/PhysRevLett.116.182501
35. R. Fossion, Study of nuclear binding energies and shape coexistence using algebraic methods. PhD thesis, Gent University (2004)
36. M. Honma, T. Otsuka, T. Mizusaki, M. Hjorth-Jensen, New effective interaction for f_5pg_9-shell nuclei. Phys. Rev. C **80**(6), 64323 (2009). https://doi.org/10.1103/PhysRevC.80.064323
37. E. Caurier, F. Nowacki, Present status of shell model techniques. Acta Phys. Pol., B **30**, 705–713 (1999)
38. B.A. Brown, W.D.M. Rae, The Shell-Model Code NuShellX@MSU. Nucl. Data Sheets **120**, 115–118 (2014). https://doi.org/10.1016/J.NDS.2014.07.022